Inverse determination of the influence of fire on vegetation carbon turnover in the pantropics

Inverse determination of the influence of fire on vegetation carbon turnover in the pantropics

Jean-François Exbrayat[1], T. Luke Smallman[1], A. Anthony Bloom[2], Lindsay B. Hutley[3], and Mathew Williams[1]

[1] National Centre for Earth Observation and School of GeoSciences, University of Edinburgh, Edinburgh, EH9 3FF, UK

[2] Jet Propulsion Laboratory, California Institute of Technology, Pasadena, California, USA

[3] Research Institute for the Environment and Livelihoods, Charles Darwin University, NT, 0909, Australia

Corresponding author: Jean-François Exbrayat (j.exbrayat@ed.ac.uk)

Key Points:

- Pixel-wise inverse modelling approach to determine the impact of fire on pantropical ecosystems functional properties
- Mean annual burned fraction correlates with increased productivity, more carbon allocated to structural pools and shorter transit times
- Large-scale patterns of shifts in allocation are in agreement with field observations which points to the need to refine parameterizations

This article has been accepted for publication and undergone full peer review but has not been through the copyediting, typesetting, pagination and proofreading process which may lead to differences between this version and the Version of Record. Please cite this article as doi: 10.1029/2018GB005925

Abstract

Fire is a major component of the terrestrial carbon cycle that has been implemented in most current global terrestrial ecosystem models (TEMs). Here, we use terrestrial carbon cycle observations to characterize the importance of fire regime gradients in the spatial distribution of ecosystem functional properties such as carbon allocation, fluxes, and turnover times in the tropics. A Bayesian model-data fusion approach is applied to an ecosystem carbon model to derive the posterior distribution of corresponding parameters for the tropics from 2000 to 2015. We perform the model-data fusion procedure twice, i.e. with and without imposing fire. Gradient of differences in model parameters and ecosystem properties in response to fire emerge between these experiments. For example, mean annual burned fraction correlates with an increase in carbon use efficiency and reductions in carbon turnover times. Further, our analyses reveal an increased allocation to more fire-resistant tissues in the most frequently burned regions. As fire modules are increasingly implemented in global TEMs, we recommend that model development includes a representation of the impact of fire on ecosystem properties as they may lead to large differences under climate change projections.

1 Introduction

Terrestrial ecosystems offset climate change by capturing and storing 25-30% of fossil-fuel emissions of carbon dioxide (Le Quéré et al., 2015), albeit with a large inter-annual variability that is driven by climate variability and fire disturbance (van der Werf et al., 2010; Reichstein et al., 2013). While terrestrial ecosystem models (TEMs) initially represented the impact of climate conditions on ecosystem carbon cycling, recent models have included the representation of fire (Hantson et al., 2016). These new features range from simpler models that use observed fire masks to prescribe burning of steady-state pools (e.g. van der Werf et al., 2010) to fully prognostic process-based models that simulate ignition and spread as a function of soil moisture (a surrogate for fuel curing), wind speed and lightning occurrences (e.g. Lenihan et al., 1998; Thonicke et al., 2010). As large fire-prone savanna regions are a major component of the global land carbon inter-annual variability (Poulter et al., 2014; Ahlström et al., 2015; Liu et al., 2015), this range of complexity in the parameterization of fire-related ecosystem properties (e.g. combustibility, survival strategies) may introduce further uncertainty and biases in estimates of the land carbon sink that remains to be quantified (Hantson et al., 2016; Rabin et al., 2017; Whitley et al., 2017).

Ecosystem models often rely on a discrete categorization of the land surface into plant functional types (PFTs). Each PFT is associated with a set of space and time-invariant parameter values that regulate the ecosystem's biogeophysical and biogeochemical responses to environmental drivers. The spatial distribution of each PFT is based on *apriori* biogeography (e.g. boreal, temperate, tropical), leaf morphology (e.g. broadleaf, needleleaf), deciduousness (deciduous or evergreen), photosynthetic pathways (C3 or C4 plants) and tree cover fraction, from grasslands to forests (Ustin & Gamon, 2010). The model-specific distribution of PFTs is usually created from land cover maps such as the MODIS-derived classification (Friedl et al., 2002) to which various levels of aggregation may be applied to reflect specific adaptation to climatic conditions (e.g. Harper et al., 2016). For example, models that participated in the fifth phase of the Coupled Model Intercomparison Project (CMIP5; Taylor et al., 2012), presented by Arora et al. (2013), represented between 5 and 16 PFTs.

The PFT approach assumes that model parameters are transferable globally within the same PFT (Kuppel et al., 2014). This involves a risk of biases due to possible over-fitting to available training datasets (Scheiter et al., 2013) which may not be representative of all possible trait values among ecosystems included within the same PFT (Verheijen et al., 2013; Scheiter et al., 2013). Indeed, TEM calibration is often performed against eddy-covariance tower data (e.g. Kuppel et al., 2014) but the spatial distribution of these datasets means that models are better constrained in temperate regions of the northern hemisphere. Another issue is that most eddy-covariance towers are installed in fire-free regions or report on fire-free periods. Therefore, models calibrated against these data will not be able to represent the observed impact of fire on ecosystem functional properties (Bond & Keeley, 2005; Pausas & Schwilk, 2012) and limitations on biomass accumulation (Murphy et al., 2014). There is a risk of over-fitting data when transferring model parameters from fire-free conditions to regions of high fire frequency. Indeed, to our knowledge only few models (e.g. aDGVM: Scheiter et al., 2013; LPX: Kelley et al., 2014) represents fire adaptation strategies identifiable in the field such as shifts in carbon allocation among plant tissues (Gignoux et al., 1997) and carbon costs associated with re-sprouting and recovery.

Introducing spatial variation in some parameters can improve the overall quality of large-scale simulations of biomass and productivity, as was demonstrated by Castanho et al., (2013) in the Amazon basin. They used in situ observations to derive relationships (i)

between net primary productivity (NPP) allocation to leaves and roots and soil sand content and (ii) between phosphorus content and maximum carboxylation capacity of RuBisCO. As a result, their model was able to reproduce gradients in woody NPP and above-ground biomass (AGB) more accurately than using homogeneous parameter values for the whole basin. Similar to this previous study (Castanho et al., 2013), we expect that spatially distributed information on ecosystem properties response to fire regimes can improve the representation of the carbon cycle in global scale TEMs but corresponding large-scale datasets are not readily available. Indeed, unlike leaf properties (Usting and Gamon, 2010), internal processes like allocation and transit times (Carvalhais et al., 2014; Bloom et al., 2016) cannot be remotely sensed and need to be retrieved through model-data fusion.

In this study, we seek to overcome this limitation by merging Earth observations of the biosphere with a process-based ecosystem model. The aim of this inverse approach is to identify spatial variation in ecosystem functional properties that are linked to fire. We focus on tropical ecosystems which feature fire-prone regions experiencing largely different disturbance regimes as represented by the spatial distribution of mean annual burned fraction (MABF; Figure 1) calculated from the Global Fire Emissions Database version 4 (GFED4; Giglio et al., 2013), the inverse of the fire return period (Li, 2002). We hypothesise that gradients in fire disturbance have significant impacts on the spatial distribution of ecosystem properties related to productivity, plant allocation and carbon turnover times (Bond and Keeley, 2005). This would point to the need to take the spatial distribution of fire regimes into account when introducing complex fire modules into TEMs.

We use the Carbon Data Model Framework (CARDAMOM; Bloom and Williams, 2015; Bloom et al., 2016) to characterise the importance of ecosystem response to fire in simulations of pantropical carbon dynamics. CARDAMOM is used to retrieve maps of model parameters corresponding to ecosystem functional properties and land-atmosphere carbon fluxes across the pantropical region in agreement with time series of fire (burned area), meteorology and remote-sensing observations of the biosphere. Erb et al. (2016) examined the impact of land-use on global biomass turnover and we take a similar approach to perform a second experiment that excludes the impact of fire on the biosphere. We thereby derive hypothetical maps of potential ecosystem properties and fluxes without fire. Comparing these two retrievals (with and without fire) allows us to quantify the influence of fire on terrestrial C balance of the pantropical region. Finally, we perform a synthetic climate change experiment to assess the impact of including or excluding fire on the sensitivity of terrestrial ecosystems to warming and increasing atmospheric CO_2.

2 Materials and Methods

2.1 CARDAMOM

CARDAMOM is a model-data fusion tool that constrains an ecosystem model with available observational datasets. It consists of two main components described hereafter: a terrestrial ecosystem model coupled with a model-data fusion procedure.

2.1.1 DALEC ecosystem model

CARDAMOM uses the Data-Assimilation Linked Ecosystem Carbon Model (DALEC; Williams et al., 2005; Bloom and Williams, 2015), a model of the terrestrial carbon cycle (Figure 2). DALEC calculates Gross Primary Production (GPP) with the Aggregated Canopy Model (ACM; Williams et al., 1997). Autotrophic respiration (R_a) is a fixed fraction of GPP and fixed fractions of the remaining Net Primary Productivity (NPP) are allocated to 4 live biomass pools: foliar, labile, wood and fine roots. The labile pool (C_{labile}) represents a

reserve of non-structural carbon that can supplement the allocation to the foliar pool (C_{foliar}) corresponding to leaf expansion. Leaf growth is controlled by a Growing Season Index (GSI), similar to the one introduced by Jolly et al. (2005).

In our model, GSI is the product of 3 piece-wise linear functions of average daily minimum temperature (T_{min}), photoperiod, and Vapour Pressure Deficit (VPD). Each of these functions returns a value that ranges from 0 (limiting conditions) to 1 (optimal conditions) and their shape is controlled by two parameters that correspond to critical values. The value of GSI is used to scale the release of C_{labile} into C_{foliar} when environmental conditions are good for leaf production. Conversely, the value (1-GSI) is used to scale leaf loss into the litter pool (C_{litter}). First-order kinetics are used to simulate the turnover of fine root C (C_{root}) into C_{litter} and woody carbon (C_{wood}) into soil organic matter carbon pool (C_{som}). Microbial decomposition produces heterotrophic respiration (R_h) and the model provides the Net Ecosystem Exchange (NEE) as the net biogenic flux of carbon from the land to the atmosphere: (calculated as $NEE = R_a + R_h - GPP$).

Fire generates carbon emissions from combustion of live and dead C pools (red upward arrows in Figure 2) but also accelerates the turnover of live carbon into dead pools (red lateral arrows in Figure 2). It is imposed to a fraction of each pixel according to the satellite-based GFED4 burned area product (Giglio et al., 2013). Fire-induced emissions and mortality fluxes are calculated similarly to van der Werf et al. (2010) with fixed combustion resilience and emissions factors of the different carbon pools (Bloom et al., 2016). At each time-step *t* emission factors k_p are used to calculate C emissions from each pool *p* due to fire such as

$$FE_{p,t} = B_t \times k_p \times C_{p,t} \qquad (1)$$

where $FE_{p,t}$ is the total fire C emission at time step t, B_t is the GFED4-derived fraction of pixel burned, and $C_{p,t}$ is the C in pool *p* at time step *t*. We use the same combustion factors as Bloom et al. (2016) for C_{labile} (0.1), C_{foliar} (0.9), C_{root} (0.1), C_{wood} (0.1), C_{litter} (0.5) and C_{som} (0.01) where higher values of k_p are used for more flammable C pools. A resilience factor r = 0.5 is assigned to simulate mortality of live biomass and C_{litter} transfer to C_{som} such as

$$FM_{p,t} = B_t \times (1 - k_p) \times (1 - r) \times C_{p,t} \qquad (2)$$

where $FM_{p,t}$ is the fire-imposed mortality or litter transfer C flux from pool p. Overall fire accelerates vegetation turnover and provides an additional input of dead organic matter in C_{som}. Fire fluxes are used to update pool sizes at each time-step and the Net Biome Exchange of C (NBE) is calculated by adding fire C emission fluxes to NEE.

2.1.2 Model-data fusion

The reduced complexity of the DALEC ecosystem model enables it to perform computationally intensive data-assimilation procedures to quantify the uncertainty in the six initial pool conditions and 20 process parameters (see Table 1) according to observations. CARDAMOM adopts the approach described in Bloom and Williams (2015) and Bloom et al. (2016) that combines a Markov Chain Monte Carlo (MCMC) procedure with Ecological and Dynamical Constraints (EDCs). The EDCs represent a formulation of the ecological common-sense that help constrain inter-dependencies between ecosystem processes (Bloom and Williams, 2015). They help reduce the uncertainty in model parameters by dismissing simulations that do not satisfy a range of conditions applied to carbon turnover rates, allocation ratios and trajectories of carbon pools. For this study, the model-data fusion procedure is performed for the pantropics using 5,417 pixels at a 1°×1° spatial resolution corresponding to the extent of the above ground biomass map from Avitabile et al. (2016).

This dataset blends two previous pantropical biomass maps (Saatchi et al., 2011; Baccini et al., 2012) with additional in-situ data and high resolution local maps. Avitabile et al. (2016) AGB map yields lower estimates of pantropical AGB stocks and different spatial patterns. Most noticeably, it predicts more biomass in the Congo basin, the Guyana shield and South-East Asia than either of Saatchi et al. (2011) or Baccini et al. (2012) maps. Conversely, Avitabile et al. (2016) maps estimates lower biomass in African savannahs and Central America.

In each pixel, the MCMC relies on Bayesian inference to determine the probability distribution of a model parameter set x given observations O such as

$$p(x|O) \propto p(x) \times p(O|x) \qquad (3)$$

where p(x) represents the prior probability of a parameter set xi calculated such as

$$p(x) = p_{EDC}(x) \times e^{-0.5\left(\frac{\log(f_{auto})-\log(0.5)}{\log(1.2)}\right)^2} \times e^{-0.5\left(\frac{\log\left(C_{eff}\right)-\log(17.5)}{\log(1.2)}\right)^2} \qquad (4)$$

with $p_{EDC}(x)$ representing the prior parameter probability according to 12 EDCs. These represent qualitative constraints to estimate realistic allocation parameters, relative turnover rates and pool trajectories in agreement with ecological knowledge. We use the same EDCs as in Bloom et al. (2016) modified from Bloom and Williams (2015). According to equation 4, p(x) also includes a prior value of 0.5 for the autotrophic respiration fraction f_{auto} (i.e. a 0.5 ratio of NPP to GPP) and a prior value of 17.5 for the canopy efficiency C_{eff}, a replacement of the nitrogen × nitrogen use efficiency product which scales GPP in ACM. These priors and their uncertainty were derived by Bloom et al. (2016) and represent the range of f_{auto} reported by DeLucia et al. (2007) and yield global GPP values consistent with Beer et al. (2010).

The likelihood p(O|x) is computed according to the ability of the model to reproduce time series of MODIS LAI fluxes and assuming that total biomass (i.e. the sum of C_{foliar}, C_{litter}, C_{root} and C_{wood}) from Avitabile et al. (2016) and C_{som} from the Harmonized World Soil Database version 1.21 (Food and Agricultural Organization, 2012) are representative of the system's initial pool sizes such as

$$p(O|x) = e^{-0.5\left(\frac{\log(O_{TBC})-\log(M_{TBC,0})}{\log(1.5)}\right)^2} \times e^{-0.5\left(\frac{\log(O_{som})-\log(M_{som,0})}{\log(1.5)}\right)^2} \times e^{-0.5\sum_{t=1}^{N}\left(\frac{\log(O_{LAI,t})-\log(M_{LAI,t})}{\log(2)}\right)^2} \qquad (5)$$

where O_{TBC} and $M_{TBC,0}$ are the observed and modelled initial total biomass carbon, O_{som} and $M_{som,0}$ are the observed and modelled initial soil organic matter carbon stocks and $O_{LAI,t}$ and $M_{LAI,t}$ are the observed and modelled LAI at time step t. Both biomass, C_{som} and LAI datasets were re-gridded to the centre of the nearest neighbour 1° × 1° pixel, using an area-weighted interpolation for biomass carbon and LAI and the dominant soil type for C_{som} as provided by Exbrayat et al. (2014). We used log-transformed values and uncertainty factors as per Bloom et al. (2016).

2.2 Characterising the influence of fire on ecosystem properties

In order to estimate the impact of fire on ecosystem properties we set up two CARDAMOM experiments over all regions covered in Avitabile et al. (2016) biomass map (Figure 1). The experiments are performed with a monthly time-step from January 2000 to

December 2015 using the ERA-Interim re-analysis climate data (Dee et al., 2011). The first experiment, hereafter referred to as FIRE, uses monthly burned area from GFED4 (Giglio et al., 2013) to impose fire on ecosystems, while we omit this driver in the second experiment (hereafter referred as NOFIRE). Apart from this difference in disturbance drivers, both experiments are identical. For each 1° × 1° grid cell, we run three MCMC chains run until 10,000,000 parameter sets have been accepted. Based on 500 parameter sets from the second half of each chain, we re-run the model 1,500 times and derive corresponding time series of ecosystem carbon fluxes and pool changes with corresponding confidence intervals. We repeat this procedure for the FIRE and NOFIRE experiments independently resulting in the retrieval of two unique parameter ensembles for every location (i.e. one with fire and one without).

CARDAMOM performs the data-assimilation procedure in each pixel without any prior information on a specific land cover or PFT although such information may exist in the data constraints such as MODIS LAI. Therefore, CARDAMOM creates smooth maps of process parameters which correspond to ecosystem functional properties (e.g. allocation of GPP to plant tissues, turnover rates). The MCMC approach estimates posterior distributions of parameter and state variables from which confidence intervals can be sampled.. We compare the FIRE and NOFIRE experiments against other datasets. We use GPP estimates from FLUXCOM (Tramontana et al., 2016; Jung et al., 2017) that correspond to up-scaled measurements from the FLUXNET network of eddy-covariance towers (Baldocchi et al., 2001; Baldocchi et al. 2014). We use the average of an ensemble of six FLUXCOM GPP datasets, each based on a different machine-learning method, to compare with our retrievals. While our estimates used GFED4's burned area as a driver, we compare the magnitude of the corresponding C emissions with those reported in GFED4 database, which are based on an ecosystem model at steady-state (van der Werf et al., 2010). Finally, we investigate the impact of introducing fire drivers on the median, i.e. highest confidence, of our retrievals as well as its impact on the uncertainty represented by the 90% confidence interval (CI_{90}). We focus on land-atmosphere fluxes, allocation of GPP into vegetation C pools and turnover times calculated following Bloom et al. (2016) such as

$$TT_p = \frac{C_P}{F_{in,p} - \Delta C_p} \qquad (6)$$

where TT_p is the turnover time (in years) of C in the p-th pool (Figure 2), C_j is the mean pool size, $F_{in,p}$ is the mean annual input into C_p due to productivity (in plant C pools C_{foliar}, C_{labile}, C_{root}, C_{wood}), turnover and fire-induced mortality (from plant pools to C_{litter} and C_{som}) and decomposition (C_{litter} to C_{som}) and ΔC_p is the mean annual change of C_p.

3 Results

3.1 Carbon balance

Both FIRE and NOFIRE experiments indicate that the pantropics were a net sink (negative NBE) of atmospheric carbon during the study period (Table 2). However, the apparently similar values of NBE in the two experiments is the result of differences in the gross fluxes that are imposed by the representation or omission of fire processes in FIRE and NOFIRE experiments, respectively. Indeed, while the sign and magnitude of NBE is similar in both experiments, NEE retrieved in the FIRE experiment indicate a stronger net carbon uptake (NEE, NBE) from tropical ecosystems than the NOFIRE experiment.

We compare retrievals with independent gridded estimates of the terrestrial carbon balance. FLUXCOM GPP estimates over the study region represent 86.6 Pg C y^{-1}, which is

about 5% lower than the median of our retrievals (Table 2). We note a tendency for CARDAMOM to simulate higher GPP than FLUXCOM at low latitudes, and the opposite at mid-latitudes of the southern hemisphere (Figure S1). Nevertheless, FLUXCOM estimates lie within the 50% confidence interval reported in Table 2 and there is a good agreement ($r = 0.88$; $p << 0.001$) in the spatial distribution of GPP in both the experiments compared to the FLUXCOM estimates.

We also compare emissions from fire retrieved in the FIRE experiment with estimates from the GFED4 database. We retrieve mean annual fire emissions of 1.18 Pg C y^{-1} which is 7% lower than the GFED4 estimate of 1.27 Pg C y^{-1}, although this number lies within the 50% confidence interval of the retrievals. There are regional differences in the distribution of fire emissions between the FIRE experiment and GFED4 emissions. Overall, CARDAMOM simulates lower emissions than GFED4 in regions located at the edge of tropical rainforests in South America, central Africa and South East Asia (i.e tropical savanna), while it simulates higher emissions in semi-arid regions of the Sahel, southern Africa and Australia. There is a significant correlation in the spatial distribution of the emissions reported by GFED4 emissions and those in the FIRE experiment ($r = 0.65$; $p << 0.001$).

3.2 Impact of fire on ecosystem properties

Clear differences in the spatial distribution of ecosystem properties emerge between the FIRE and NOFIRE simulations. In most locations, annual GPP is higher in the FIRE simulations compared to the NOFIRE simulations (Figure 3a). This difference is exacerbated in areas where MABF is large, leading to differences up to 0.1 kg C m^{-2} y^{-1} (Figure 3a), or a 6% increase of GPP in the FIRE experiment compared to the NOFIRE experiment where MABF is >10%. The increase in retrieved GPP in FIRE is accompanied by a decrease in R_{eco} (Figure 3b). The reduction of R_{eco} in FIRE compared to NOFIRE follows a trend with MABF (Figure 3b) and it decreases by about 5% in areas where MABF is >10%. We do not identify a change in the uncertainty of the GPP and R_{eco} retrievals as represented by the width of the CI_{90} (Figure 3c and 3d).

Similar to GPP, imposing fire disturbances led FIRE retrievals to estimate stronger pantropical NPP than in NOFIRE retrievals (Table 2). The distribution of the increase in NPP follows a pattern similar to the increase in GPP. Compared to the NOFIRE simulations, places with the highest MABF exhibit the strongest increase in median NPP (Figure 4a) in the FIRE simulation that is on average 10% where MABF is >10%. The higher NPP in the FIRE experiment is due to higher GPP, lower R_a (Table 2) and an increase in carbon-use efficiency (CUE, NPP/GPP; Figure 4b and 4c). The increase in CUE in the FIRE simulation is stronger in regions where the MABF is high (Figure 4b and 4c). CUE is on average 4% higher in the FIRE simulation than in the NOFIRE simulation where MABF is >10%. Additional to the increase in CUE, imposing fire leads to changes in NPP allocation, with shift toward a smaller fraction of NPP allocated to photosynthetic C pools (i.e. foliar and labile pools; Figure 4b) and, conversely, a bigger fraction of NPP allocated to structural C pools (i.e. wood and root pools; Figure 4c). The magnitude of the changes in NPP allocation patterns is relative to MABF. In places where it is >10%, FIRE retrievals allocate on average an 8% smaller fraction of NPP to photosynthetic C pools, and a 22% greater fraction to structural C pools.

FIRE simulations estimate a biomass of 300.2 (232.0 / 391.2) Pg C in the study area, which is 2.5% lower than the corresponding estimate of 307.4 (236.7 / 402.4) Pg C in NOFIRE simulations. While the difference is marginal at the pantropical scale, we note that there is a tendency for a reduction in vegetation biomass in regions where fire regime is

intense (Figure 5a and 5c), particularly in central Africa and Australia. This is accompanied by a reduction in uncertainty that follows the same tendency (Figure 5b and 5d). On average, in regions where MABF is >10% the median biomass retrieved in the FIRE experiment is 16% lower than that in NOFIRE while the corresponding uncertainty shrinks by 29%. This occurs despite using the same prior for biomass derived from Avitabile et al. (2016) in both experiments (Figure S3). For the whole pantropics the median NOFIRE retrievals of biomass are in better agreement (Figure S3b; rmse ≈ 0.389 kg C m^{-2}) with the prior than the FIRE retrievals (Figure S3a; rmse ≈ 0.477 kg C m^{-2}). Furthermore, the difference between FIRE retrievals and observations from Avitabile et al. (2016) grows for greater MABF (Figure S3a) while NOFIRE retrievals are comparable to the prior from Avitabile et al. (2016) across the whole pantropics (Figure S3b).

The increase in NPP and reduction of biomass lead retrieved vegetation carbon transit times to be shorter in the FIRE experiment compared to the NOFIRE experiment (Figure 6a) especially in regions where MABF is large (Figure 6c). Over the whole pantropical region imposing fire leads to an area-weighted 7% acceleration of vegetation carbon cycling corresponding to a shortening of area-weighted transit time from 8.5 years to 7.9 years. It drives a 3% shortening of highest confidence average ecosystem carbon transit times shifting from 38.9 years in NOFIRE to 37.6 years in FIRE. However, the spatial distribution of these differences is heterogeneous and matches regions where MABF is the highest, especially southern Africa and northern Australia (Figure 6a). In places where MABF is >10%, the area-weighted median vegetation carbon turnover time retrieved by CARDAMOM is 32% shorter in the FIRE simulations compared to the NOFIRE simulations. This tendency toward a reduction of the vegetation carbon turnover times in frequently burned pixels is mirrored by a reduction in the uncertainty of the retrievals (Figure 6b and 6d). Compared to the NOFIRE experiment, the uncertainty in the FIRE retrievals of vegetation carbon turnover time, measured as the width of the 90% confidence interval, is reduced by 7% over the whole pantropical regions. However, similarly to the median retrievals, the main impact is seen in regions with a high frequency of fire, and a mean reduction of the uncertainty by 48% in pixels where MABF > 10% (Figure 6d).

4 Discussion

We have retrieved the modern terrestrial carbon cycle in the pantropics using two alternative model versions that include or omit fire processes imposed by observations of burned area (Giglio et al., 2013). We note that both experiments yield similar results in pantropical GPP. Still, we note that pantropical GPP increases in the FIRE experiment which is mostly due to an increase in regions with larger MABF (Figure 3a) where growth and recovery are stimulated even in places where LAI may have been largely reduced. Higher productivity in retrievals that include fire may seem counter-intuitive as it is a globally significant consumer but these results were not unexpected considering several aspects of the inverse model-data fusion approach we adopted. For example, GPP is constrained through the assimilation of the same LAI time series in the ACM model (Williams et al., 1997) and the use of the same prior value for the parameter C_{eff} (Table 1; Bloom et al., 2016) in both experiments. Therefore, both retrievals yield similar values but productivity is higher in FIRE to offset LAI losses due to fire. In both experiments the highest confidence estimates agree that the pantropical regions have acted as a sink of atmospheric CO_2 of 1.7 Pg C y^{-1} in the FIRE experiment and 1.9 Pg C y^{-1} in the NOFIRE experiment. These comparable estimates are due to a stronger biogenic sink (i.e. more negative NEE; Table 2) in the FIRE experiment that is partially offset by fire emissions. The similarity between NBE retrievals obtained with and without prescription of fire can be attributed to the use of the same biomass and soil

carbon constraints with corresponding EDCs designed to limit the drift of carbon pools. Overall, similarities in the simulated pantropical carbon balance were expected but the inverse model-data fusion approach highlights differences in inner dynamics imposed by the addition or omission of fire disturbances.

Compared to GFED4 the FIRE experiment yields systematically higher emissions in semi-arid regions, and conversely less in more humid regions. Differences in fire emissions between the FIRE experiment and the GFED4 estimates (Figure S2) may arise from differences in the way fire is imposed, and carbon stocks and associated combustion factors at the time fire occurs. The GFED4 (van der Werf et al., 2010) fire C loss approach distinguishes between herbaceous, forest and peat fires and sub-grid scales, which effectively introduces spatially-explicit patterns in the GFED combustion factors. In contrast, DALEC combustion factors are assumed to be constant throughout the tropics while observational studies indicate they may vary spatially and temporally (Russell-Smith et al. 2009). This current limitation in DALEC could lead to relatively higher fire C emissions in grid-cells comprised of both forest, savanna and grassland ecosystems, but where fires predominantly occur within the savanna and grassland regions (Giglio et al., 2013). Furthermore, van der Werf et al. (2010) limit the soil C loss to 50cm in biomass burning regions, while CARDAMOM soil pool depth is not resolved. It points to a possible overestimation of emissions from DALEC as controlled fire experiments indicate that low intensity fires do not have significant impacts on soil processes in frequently burned savannas of South America (Pinto et al., 2002), southern Africa (Zepp et al., 1996) and Australia (Livesley et al., 2011). Differences between CARDAMOM and GFED, as well as the wide range of combustion factor estimates across tropical ecosystems (Ward et al., 1997; Carvalho et al., 2001; van Leeuwen et al., 2014, amongst many others) highlight that further efforts are needed to establish the sensitivity of our results to prescribed fire combustion factors. Following this study, developments of DALEC will address this aspect by dynamically linking combustion factors to the ecosystem water balance, assuming higher combustibility under dry conditions. Additional drivers like fire radiative power (Freeborn et al., 2014) could also be used to constrain combustion completeness.

Another notable difference between GFED and CARDAMOM fire emissions is that the assimilated biomass map values (Avitabile et al., 2016) – which exhibit the effects of past deforestation – constrain the initial carbon pools: in contrast, GFED4 estimates rely on a model brought to equilibrium by recycling modern climate and fire burned area data (van der Werf et al., 2010). Therefore, our estimates have less fuel to burn in these areas and that partially explains the systematically lower emissions simulated by CARDAMOM in the wet tropics at the edge of the rainforests (Figure S2). We note that the uncertainty in CARDAMOM's estimates may be seen as a current limitation, but we are confident that the future availability of high frequency remotely-sensed biomass data (e.g. Le Toan et al., 2011) will help improve its ability to estimate the state and dynamics of the terrestrial carbon cycle as shown with site-scale experiments (Smallman et al., 2017).

The impact of fire on land-atmosphere carbon fluxes and transit times is reflected by changes in plant allocation patterns between NOFIRE and FIRE simulations. For more frequently burned ecosystems, there was an increased allocation of NPP to structural C (i.e. C_{wood} and C_{roots}; Figure 4c) at the expense of photosynthetic C (i.e. C_{foliar} and C_{labile}; Figure 4b). This model behaviour is similar to the increased allocation of carbon to fire resistant bark after imposing fire in the experiment reported by Scheiter et al. (2013) and observations of Lawes et al. (2011a) on fire resistance conferred by bark thickness. Comparing retrievals from the FIRE and NOFIRE experiments, we note a strong influence of fire on ecosystem fluxes and functional properties. At the pantropical scale, feedbacks between fire and

biogenic processes in the FIRE experiment maintain a carbon balance similar to the NOFIRE experiment. This is explained by the interplay between adjusted allocation and turnover rates that increase the capacity of plants to store C (NEE in Table 2) and high levels of sequestration post-fire recovery in the corresponding experiments. Regional differences between the FIRE and NOFIRE experiment indicate a coupling of higher productivity, higher CUE and allocation to resistant plant parts with more intense fire regimes (Figure 4). We note a shortening in vegetation and ecosystem C transit times when imposing fire, clearly linked to disturbance and resulting C losses followed by rapid regrowth associated with the modelled increase in GPP in intensely burned regions (Figure 3).

The reduction of biomass (Figure 5) for higher MABF agrees with aDGVM model simulations of fire suppression over African savannas (Scheiter and Higgins, 2009) and fire management for northern Australia (Scheiter et al., 2015) as well as worldwide observations from in-situ fire exclusion experiments (Tilman et al., 2000; Higgins et al., 2007). Furthermore, the larger decrease in biomass from the NOFIRE to the FIRE simulations is in agreement with observations that indicated a negative correlation between fire frequency and biomass in Australian tropical savannas for example (Williams et al., 1999; Russell-Smith et al., 2003; Murphy et al., 2014). There is also an increase in differences between prior biomass information and values retrieved in the FIRE experiment as MABF increases (Figure S3). The lack of agreement between our retrievals and prior biomass data indicates that relevance of pan-tropical biomass maps for model benchmarking in fire-prone regions needs to be evaluated.

Clear shifts in CUE and plant carbon allocation in response to fire emerge between the FIRE and NOFIRE experiments (Figure 4). CUE increases in fire-prone regions already capable of high GPP (Figure 3), which results in higher NPP (Figure 4a) and thus providing more carbon available to drive re-sprouting and/or coppicing and stand regeneration post fire (Beringer et al. 2007). Ecosystems with higher MABF invest less in 'easily burned tissues' (i.e. leaves; Figure 4b) and more in fire resistant tissues (i.e. woody C in our model; Figure 4c). Such a resistance strategy is evident in woody vegetation in fire-prone ecosystems of Australian (Clarke et al., 2015, Lawes et al. 2011b) and African savannas (Gignoux et al., 1997; Nefabas and Gambiza, 2007) and also emerges from individual-based modelling (Scheiter et al., 2013). Indeed, allocating carbon to less flammable plant pools results in a reduction of fuel loads and an increase in survival chances (Clarke et al., 2013). The capacity for CARDAMOM to retrieve parameter sets representing shifts in ecosystem properties in response to changes in MABF leads to reduced uncertainty of retrieved ecosystem stocks and turnover times (Figure 5 and 6) although few outliers exhibit the opposite behavior in regions of the Sahel where MABF is between 20% and 50%. While we do not investigate this aspect further we suspect that it might come from the mix of natural and managed fires in this region. In every other places, fire strongly constrains ecosystem carbon pathways and turnover processes during the assimilation procedure.

Our large-scale results are in agreement with field observations of the influence of fire on ecosystem functional properties (Pausas and Schwilk, 2011). While our approach is currently focused on the tropics, we expect similar relationships to emerge in temperate and boreal ecosystems. However, the lack of availability of a wall-to-wall biomass maps in extra-tropical regions currently limits the applicability of our approach. A similar investigation will be made possible by the upcoming launch of the Global Ecosystem Dynamics Investigation (GEDI; Stavros et al., 2017) which should provide a global biomass map in 2020. The parameter and transit time maps (Figures 3-6) indicate that fire spatially influences ecosystem functioning properties crossing boundaries between PFT maps used in classical TEMs. While PFT maps are subject to criticism, we acknowledge that they offer a trade-off between model

precision and computational costs. Therefore, for next generation TEMs to rely on distributed trait maps, further studies are required on fire-climates interactions with ecosystem parameters. For example, separating evergreen broadleaf ecosystems into two different tropical and temperate PFTs and updating parameter values to match with observational datasets of traits values (Kattge et al., 2011) has recently led to improvements in the JULES model (Clark et al., 2011; Harper et al., 2016). An option to mirror this approach with respect to fire dynamics could be to further categorize PFTs based on the distribution of fire regimes (Archibald et al., 2013; Whitley et al.; 2017). For example, Archibald et al. (2013) have identified five global syndromes of fires regimes, or pyromes, based on remotely-sensed information of their frequency, intensity and size. They showed that the spatial distribution of pyromes resulted from complex interactions between biome types, local climate and human activities, all of which may change in a warmer world.

5 Conclusions

We have used the CARDAMOM model-data fusion system to retrieve continuous parameter maps related to C cycling for the DALEC ecosystem model at one degree spatial resolution for the whole pantropics. Our coarse resolution results reveal shifts in CUE, allocation and biomass that are in agreement with field observations of the impact of fire, or of its exclusion, on ecosystem properties. The model-data fusion procedure retrieved shorter turnover times of carbon in vegetation and ecosystems when fire processes were represented. We attribute this acceleration of the turnover to an increase in NPP, driven by higher CUE, and lower biomass stocks. Additionally, there is a shift toward more allocation to fire resistant plant tissues. We note that the magnitude of differences imposed by fire gradually increases with MABF while the corresponding uncertainties shrink, indicating that fire processes imposed a strong constraint on retrieved properties. Finally, the synthetic climate sensitivity test we perform indicates non-trivial differences in the sensitivity of ecosystems to future climate change when fire disturbances were included in the model-data fusion. As prognostic fire is a process that is increasingly implemented in TEMs our results highlight the need to better represent ecosystem response to fire.

Acknowledgements

This study was supported by the Natural Environment Research Council through the National Centre for Earth Observation, contract number PR140015. This research was also supported by the Newton Fund, through CSSP Brazil. Contribution by AAB was carried out at the Jet Propulsion Laboratory, California Institute of Technology, under a contract with the National Aeronautics and Space Administration (NNH16ZDA001N-IDS). Data-assimilation procedures were performed using the Edinburgh Compute and Data Facility resources. The authors acknowledge the European Centre for Medium-Range Weather Forecasts for the availability of climate drivers, the FAO for the Harmonized World Soil Database, and NASA for MODIS data. The lead author was also supported by a Postdoctoral and Early Career Research Exchange scholarship from the Scottish Alliance for Geoscience, Environment and Society.

Data availability

CARDAMOM simulations used in this study are freely available from Exbrayat et al. (2018) on the University of Edinburgh's DataShare service: http://dx.doi.org/10.7488/ds/2317.

FLUXCOM GPP estimates used in this study are available from the data portal of the Max Planck Institute for Biogeochemistry at

https://doi.org/10.17871/FLUXCOM_RS_METEO_CRUNCEPv6_1980_2013_v1 (Jung, 2016).

GFED4 fire emissions estimates are available from http://www.globalfiredata.org

Conflicts of interest

The authors declare no conflicts of interest.

References

Ahlström, A., Raupach, M. R., Schurgers, G., Smith, B., Arneth, A., Jung, M., et al. (2015). The dominant role of semi-arid ecosystems in the trend and variability of the land CO_2 sink. Science, 348(6237), 895–899. https://doi.org/10.1126/science.aaa1668

Archibald, S., Lehmann, C. E. R., Gómez-Dans, J. L., & Bradstock, R. A. (2013). Defining pyromes and global syndromes of fire regimes. Proceedings of the National Academy of Sciences of the United States of America, 110(16), 6442–7. https://doi.org/10.1073/pnas.1211466110

Arora, V. K., Boer, G. J., Friedlingstein, P., Eby, M., Jones, C. D., Christian, J. R., et al. (2013). Carbon–Concentration and Carbon–Climate Feedbacks in CMIP5 Earth System Models. Journal of Climate, 26(15), 5289–5314. https://doi.org/10.1175/JCLI-D-12-00494.1

Avitabile, V., Herold, M., Heuvelink, G. B. M., Lewis, S. L., Phillips, O. L., Asner, G. P., et al. (2016). An integrated pan-tropical biomass map using multiple reference datasets. Global Change Biology, 22(4), 1406–1420. https://doi.org/10.1111/gcb.13139

Baldocchi, D., Falge, E., Gu, L. H., Olson, R., Hollinger, D., Running, S., et al. (2001). FLUXNET: A new tool to study the temporal and spatial variability of ecosystem-scale carbon dioxide, water vapor, and energy flux densities. Bulletin of the American Meteorological Society, 82(11), 2415–2434. https://doi.org/10.1175/1520-0477(2001)082<2415:fantts>2.3.co;2

Baldocchi, D. (2014). Measuring fluxes of trace gases and energy between ecosystems and the atmosphere - the state and future of the eddy covariance method. Global Change Biology, 20(12), 3600–3609. https://doi.org/10.1111/gcb.12649

Beringer, J., Hutley, L. B., Tapper, N. J., & Cernusak, L. A. (2007). Savanna fires and their impact on net ecosystem productivity in North Australia. *Global Change Biology*, *13*(5), 990–1004. https://doi.org/10.1111/j.1365-2486.2007.01334.x

Bloom, A. A., Exbrayat, J.-F., van der Velde, I. R., Feng, L., & Williams, M. (2016). The decadal state of the terrestrial carbon cycle: Global retrievals of terrestrial carbon allocation, pools, and residence times. Proceedings of the National Academy of Sciences of the United States of America, 113(5), 1285–1290. https://doi.org/10.1073/pnas.1515160113

Bloom, A. A., & Williams, M. (2015). Constraining ecosystem carbon dynamics in a data-limited world: integrating ecological "common sense" in a model–data fusion framework. Biogeosciences, 12(5), 1299–1315. https://doi.org/10.5194/bg-12-1299-2015

Bond, W., & Keeley, J. (2005). Fire as a global "herbivore": the ecology and evolution of flammable ecosystems. Trends in Ecology & Evolution, 20(7), 387–394. https://doi.org/10.1016/j.tree.2005.04.025

Castanho, A. D. A., Coe, M. T., Costa, M. H., Malhi, Y., Galbraith, D., & Quesada, C. A. (2013). Improving simulated Amazon forest biomass and productivity by including spatial variation in biophysical parameters. Biogeosciences, 10(4), 2255–2272. https://doi.org/10.5194/bg-10-2255-2013

Carvalhais, N., Forkel, M., Khomik, M., Bellarby, J., Jung, M., Migliavacca, M., … Reichstein, M. (2014). Global covariation of carbon turnover times with climate in terrestrial ecosystems. *Nature*, *514*(7521), 213–7. https://doi.org/10.1038/nature13731

Carvalho, J. A., Costa, F. S., Gurgel Veras, C. A., Sandberg, D. V., Alvarado, E. C., Gielow, R., et al. (2001). Biomass fire consumption and carbon release rates of rainforest-clearing experiments conducted in northern Mato Grosso, Brazil. *Journal of Geophysical Research: Atmospheres*, *106*(D16), 17877–17887. https://doi.org/10.1029/2000JD900791

Clark, D. B., Mercado, L. M., Sitch, S., Jones, C. D., Gedney, N., Best, M. J., et al. (2011). The Joint UK Land Environment Simulator (JULES), model description – Part 2: Carbon fluxes and vegetation dynamics. *Geoscientific Model Development*, *4*(3), 701–722. https://doi.org/10.5194/gmd-4-701-2011

Clarke, P. J., Lawes, M. J., Midgley, J. J., Lamont, B. B., Ojeda, F., Burrows, G. E., et al. (2013). Resprouting as a key functional trait: How buds, protection and resources drive persistence after fire. *New Phytologist*. https://doi.org/10.1111/nph.12001

Clarke, P. J., Lawes, M. J., Murphy, B. P., Russell-Smith, J., Nano, C. E. M., Bradstock, R., et al. (2015). A synthesis of postfire recovery traits of woody plants in Australian ecosystems. *Science of The Total Environment*, *534*, 31–42. https://doi.org/10.1016/j.scitotenv.2015.04.002

Dee, D. P., Uppala, S. M., Simmons, A. J., Berrisford, P., Poli, P., Kobayashi, S., et al. (2011). The ERA-Interim reanalysis: configuration and performance of the data assimilation system. *Quarterly Journal of the Royal Meteorological Society*, *137*(656), 553–597. https://doi.org/10.1002/qj.828

Erb, K. H., Fetzel, T., Plutzar, C., Kastner, T., Lauk, C., Mayer, A., et al. (2016). Biomass turnover time in terrestrial ecosystems halved by land use. *Nature Geoscience*, *9*(9), 674–678. https://doi.org/10.1038/ngeo2782

Exbrayat, J.-F., Pitman, A. J., & Abramowitz, G. (2014). Disentangling residence time and temperature sensitivity of microbial decomposition in a global soil carbon model. Biogeosciences, 11(23), 6999–7008. https://doi.org/10.5194/bg-11-6999-2014

Exbrayat, J.-F., Williams, M. & Smallman, T L. (2018) CARDAMOM pantropical retrievals 2000-2015, 2000-2015 [dataset]. *National Centre for Earth Observation and School of GeoSciences. University of Edinburgh*. https://dx.doi.org/10.7488/ds/2317

Food and Agriculture Organization, I. ISRIC, ISSCAS, and JRC (2012), *Harmonized World Soil Database (Version 1.2)*, FAO and IIASA, Rome, Italy and Laxenburg, Austria.

Freeborn, P. H., Wooster, M. J., Roy, D. P., & Cochrane, M. A. (2014). Quantification of MODIS fire radiative power (FRP) measurement uncertainty for use in satellite-based active fire characterization and biomass burning estimation. *Geophysical Research Letters*, *41*(6), 1988–1994. https://doi.org/10.1002/2013GL059086

Friedl, M. A., McIver, D. K., Hodges, J. C. F., Zhang, X., Muchoney, D., Strahler, A. H., et al. (2002). Global land cover mapping from MODIS: algorithms and early results. *Remote Sensing Of Environment*, *83*, 287–302. https://doi.org/10.1016/S0034-4257(02)00078-0

Giglio, L., Randerson, J. T., & van der Werf, G. R. (2013). Analysis of daily, monthly, and annual burned area using the fourth-generation global fire emissions database (GFED4). *Journal of Geophysical Research: Biogeosciences*, *118*(1), 317–328. https://doi.org/10.1002/jgrg.20042

Gignoux, J., Clobert, J., & Menaut, J.-C. (1997). Alternative fire resistance strategies in savanna trees. *Oecologia*, *110*(4), 576–583. https://doi.org/10.1007/s004420050198

Hantson, S., Arneth, A., Harrison, S. P., Kelley, D. I., Prentice, I. C., Rabin, S. S., et al. (2016). The status and challenge of global fire modelling. *Biogeosciences*, *13*(11), 3359–3375. https://doi.org/10.5194/bg-13-3359-2016

Harper, A Harper, A. B., Cox, P. M., Friedlingstein, P., Wiltshire, A. J., Jones, C. D., Sitch, S., et al. (2016). Improved representation of plant functional types and physiology in the Joint UK Land Environment Simulator (JULES v4.2) using plant trait information. Geoscientific Model Development, 9(7), 2415–2440. https://doi.org/10.5194/gmd-9-2415-2016

Higgins, S. I., Bond, W. J., February, E. C., Bronn, A., Euston-Brown, D. I. W., Enslin, B., et al. (2007). Effects of four decades of fire manipulation on woody vegetation structure in savanna. Ecology, 88(5), 1119–1125. https://doi.org/10.1890/06-1664

Jolly, W. M., Nemani, R., & Running, S. W. (2005). A generalized, bioclimatic index to predict foliar phenology in response to climate. *Global Change Biology*, *11*(4), 619–632. https://doi.org/10.1111/j.1365-2486.2005.00930.x

Jung, M., Reichstein, M., Schwalm, C. R., Huntingford, C., Sitch, S., Ahlström, A., et al. (2017). Compensatory water effects link yearly global land CO2 sink changes to temperature. *Nature*, *541*(7638), 516–520. https://doi.org/10.1038/nature20780

Kattge, J., Díaz, S., Lavorel, S., Prentice, I. C., Leadley, P., Bönisch, G., et al. (2011). TRY - a global database of plant traits. *Global Change Biology*, *17*(9), 2905–2935. https://doi.org/10.1111/j.1365-2486.2011.02451.x

Kelley, D. I., Harrison, S. P., & Prentice, I. C. (2014). Improved simulation of fire–vegetation interactions in the Land surface Processes and eXchanges dynamic global vegetation model (LPX-Mv1). *Geoscientific Model Development*, *7*(5), 2411–2433. https://doi.org/10.5194/gmd-7-2411-2014

Kuppel, S., Peylin, P., Maignan, F., Chevallier, F., Kiely, G., Montagnani, L., & Cescatti, A. (2014). Model–data fusion across ecosystems: from multisite optimizations to global simulations. *Geoscientific Model Development*, *7*(6), 2581–2597. https://doi.org/10.5194/gmd-7-2581-2014

Lawes, M. J., Adie, H., Russell-Smith, J., Murphy, B., & Midgley, J. J. (2011). How do small savanna trees avoid stem mortality by fire? the roles of stem diameter, height and bark thickness. Ecosphere, 2(4). https://doi.org/10.1890/ES10-00204.1

Lawes, M. J., Richards, A., Dathe, J., & Midgley, J. J. (2011). Bark thickness determines fire resistance of selected tree species from fire-prone tropical savanna in north Australia. Plant Ecology, 212(12), 2057–2069. https://doi.org/10.1007/s11258-011-9954-7

Lenihan, J. M., Daly, C., Bachelet, D., & Neilson, R. P. (1998). Simulating Broad-Scale Fire Severity in a Dynamic Global Vegetation Model. *Northwest Science*, *72*, 91–103.

Le Quéré, C., Moriarty, R., Andrew, R. M., Peters, G. P., Ciais, P., Friedlingstein, P., et al. (2015). Global carbon budget 2014. *Earth System Science Data*, *7*(1), 47–85. https://doi.org/10.5194/essd-7-47-2015

Le Toan, T., Quegan, S., Davidson, M. W. J., Balzter, H., Paillou, P., Papathanassiou, K., et al. (2011). The BIOMASS mission: Mapping global forest biomass to better understand the terrestrial carbon cycle. *Remote Sensing of Environment*, *115*(11), 2850–2860. https://doi.org/10.1016/j.rse.2011.03.020

Li, C. (2002). Estimation of fire frequency and fire cycle: A computational perspective. *Ecological Modelling*, *154*(1–2), 103–120. https://doi.org/10.1016/S0304-3800(02)00069-8

Livesley, S. J., Grover, S., Hutley, L. B., Jamali, H., Butterbach-Bahl, K., Fest, B., et al. (2011). Seasonal variation and fire effects on CH4, N2O and CO2 exchange in savanna soils of northern Australia. *Agricultural Forest and Meteorology*, *151*(11), 1440-1452. https://doi.org/10.1016/j.agrformet.2011.02.001

Liu, Y. Y., van Dijk, A. I. J. M., de Jeu, R. A. M., Canadell, J. G., McCabe, M. F., Evans, J. P., & Wang, G. (2015). Recent reversal in loss of global terrestrial biomass. *Nature Climate Change*, *5*(5), 470–474. https://doi.org/10.1038/nclimate2581

Murphy, B. P., Lehmann, C. E. R., Russell-Smith, J., & Lawes, M. J. (2014). Fire regimes and woody biomass dynamics in Australian savannas. *Journal of Biogeography*, *41*(1), 133–144. https://doi.org/10.1111/jbi.12204

Nefabas, L. L., & Gambiza, J. (2007). Fire-tolerance mechanisms of common woody plant species in a semiarid savanna in south-western Zimbabwe. *African Journal of Ecology*, *45*(4), 550–556. https://doi.org/10.1111/j.1365-2028.2007.00767.x

Pausas, J. G., & Schwilk, D. (2012). Fire and plant evolution. MEDECOS Special Session on "Fire as an evolutionary pressure shaping plant traits", Los Angeles, CA, USA, September 2011. *The New Phytologist*, *193*(2), 301–3. https://doi.org/10.1111/j.1469-8137.2011.04010.x

Pinto A. S., Bustamante, M. M. C., Kisselle, K., Burke, R., Zepp, R., Viana, L. T., et al. (2002). Soil emissions of N2O, NO, and CO2 in Brazilian Savannas: Effects of vegetation type, seasonality and prescribed fires. *Journal of Geophysical Research*, *107*(D20), 8089, https://doi.org/10.1029/2001JD000342

Poulter, B., Frank, D., Ciais, P., Myneni, R. B., Andela, N., Bi, J., et al. (2014). Contribution of semi-arid ecosystems to interannual variability of the global carbon cycle. *Nature*, *509*(7502), 600–603. https://doi.org/10.1038/nature13376

Rabin, S. S., Melton, J. R., Lasslop, G., Bachelet, D., Forrest, M., Hantson, S., et al. (2017). The Fire Modeling Intercomparison Project (FireMIP), phase 1: Experimental and analytical protocols with detailed model descriptions. *Geoscientific Model Development*, *10*(3), 1175–1197. https://doi.org/10.5194/gmd-10-1175-2017

Reichstein, M., Bahn, M., Ciais, P., Frank, D., Mahecha, M. D., Seneviratne, S. I., et al. (2013). Climate extremes and the carbon cycle. *Nature*, *500*(7462), 287–95. https://doi.org/10.1038/nature12350

Russell-Smith, J., Murphy, B. P., Meyer, C. P., Cook, G. D., Maier, S., Edwards, A. C., et al. (2009). Improving estimates of savanna burning emissions for greenhouse accounting in northern Australia: limitations, challenges, applications. International Journal of Wildland Fire, 18(1), 1. https://doi.org/10.1071/WF08009

Russell-Smith, J., Whitehead, P. J., Cook, G. D., & Hoare, J. L. (2003). Response of Eucalyptus-dominated savanna to frequent fires: Lessons from Munmarlary, 1973-1996. *Ecological Monographs*, *73*(3), 349–375. https://doi.org/10.1890/01-4021

Saatchi, S. S., Harris, N. L., Brown, S., Lefsky, M., Mitchard, E. T. A., Salas, W., et al. (2011). Benchmark map of forest carbon stocks in tropical regions across three continents. *Proceedings of the National Academy of Sciences of the United States of America*, *108*(24), 9899–9904. https://doi.org/10.1073/pnas.1019576108

Scheiter, S., & Higgins, S. I. (2009). Impacts of climate change on the vegetation of Africa: an adaptive dynamic vegetation modelling approach. *Global Change Biology*, *15*(9), 2224–2246. https://doi.org/10.1111/j.1365-2486.2008.01838.x

Scheiter, S., Higgins, S. I., Beringer, J., & Hutley, L. B. (2015). Climate change and long-term fire management impacts on Australian savannas. *New Phytologist*, *205*(3), 1211–26. https://doi.org/10.1111/nph.13130

Scheiter, S., Langan, L., & Higgins, S. I. (2013). Next-generation dynamic global vegetation models: learning from community ecology. *New Phytologist*, *198*(3), 957–69. https://doi.org/10.1111/nph.12210

Smallman, T. L., Exbrayat, J. F., Mencuccini, M., Bloom, A. A., & Williams, M. (2017). Assimilation of repeated woody biomass observations constrains decadal ecosystem carbon cycle uncertainty in aggrading forests. *Journal of Geophysical Research: Biogeosciences*, *122*(3), 528–545. https://doi.org/10.1002/2016JG003520

Stavros, E. N., Schimel, D., Pavlick, R., Serbin, S., Swann, A., et al. (2017). ISS observations offer insights into plant function. *Nature Ecology & Evolution*, *1*, 0194. https://doi.org/10.1038/s41559-017-0194

Taylor, K. E., Stouffer, R. J., & Meehl, G. A. (2012). An Overview of CMIP5 and the Experiment Design. *Bulletin of the American Meteorological Society*, *93*(4), 485–498. https://doi.org/10.1175/BAMS-D-11-00094.1

Thonicke, K., Spessa, A., Prentice, I. C., Harrison, S. P., Dong, L., & Carmona-Moreno, C. (2010). The influence of vegetation, fire spread and fire behaviour on biomass burning and trace gas emissions: Results from a process-based model. *Biogeosciences*, *7*(6), 1991–2011. https://doi.org/10.5194/bg-7-1991-2010

Tilman, D., Reich, P., Phillips, H., Menton, M., Patel, A., Vos, E., et al. (2000). Fire Suppression and ecosystem carbon storage. *Ecology*, *81*(10), 2680–2685. https://doi.org/10.1890/0012-9658(2000)081[2680:FSAECS]2.0.CO;2

Tramontana, G., Jung, M., Schwalm, C. R., Ichii, K., Camps-Valls, G., Ráduly, B., et al. (2016). Predicting carbon dioxide and energy fluxes across global FLUXNET sites with regression algorithms. *Biogeosciences*, *13*(14), 4291–4313. https://doi.org/10.5194/bg-13-4291-2016

Ustin, S. L., & Gamon, J. A. (2010). Remote sensing of plant functional types. *New Phytologist*, *186*(4), 795–816. https://doi.org/10.1111/j.1469-8137.2010.03284.x

van der Werf, G. R., Randerson, J. T., Giglio, L., Collatz, G. J., Mu, M., Kasibhatla, P. S., et al. (2010). Global fire emissions and the contribution of deforestation, savanna, forest, agricultural, and peat fires (1997–2009). *Atmospheric Chemistry and Physics*, *10*(23), 11707–11735. https://doi.org/10.5194/acp-10-11707-2010

van Leeuwen, T. T., van der Werf, G. R., Hoffmann, A. A., Detmers, R. G., Rücker, G., French, N. H. F., et al. (2014). Biomass burning fuel consumption rates: a field measurement database. *Biogeosciences*, *11*(24), 7305–7329. https://doi.org/10.5194/bg-11-7305-2014

Verheijen, L. M., Brovkin, V., Aerts, R., Bönisch, G., Cornelissen, J. H. C., Kattge, J., et al. (2013). Impacts of trait variation through observed trait–climate relationships on performance of an Earth system model: a conceptual analysis. *Biogeosciences*, *10*(8), 5497–5515. https://doi.org/10.5194/bg-10-5497-2013

Ward, D. E., Hao, W. M., Susott, R. a., Babbitt, R. E., Shea, R. W., Kauffman, J. B., & Justice, C. O. (1996). Effect of fuel composition on combustion efficiency and emission factors for African savanna ecosystems. *Journal of Geophysical Research*, *101*(D19), 23569. https://doi.org/10.1029/95JD02595

Whitley, R., Beringer, J., Hutley, L. B., Abramowitz, G., De Kauwe, M. G., Evans, B., et al. (2017). Challenges and opportunities in land surface modelling of savanna ecosystems. *Biogeosciences*, *14*(20), 4711–4732. https://doi.org/10.5194/bg-14-4711-2017

Williams, M., Rastetter, E. B., Fernandes, D. N., Goulden, M. L., Shaver, G. R., & Johnson, L. C. (1997). Predicting gross primary productivity in terrestrial ecosystems. *Ecological Applications*, *7*(3), 882–894. https://doi.org/10.1890/1051-0761(1997)007[0882:PGPPIT]2.0.CO;2

Williams, M., Schwarz, P. A., Law, B. E., Irvine, J., & Kurpius, M. R. (2005). An improved analysis of forest carbon dynamics using data assimilation. *Global Change Biology*, *11*(1), 89–105. https://doi.org/10.1111/j.1365-2486.2004.00891.x

Williams, R. J., Cook, G. D., Gill, A. M., & Moore, P. H. R. (1999). Fire regime, fire intensity and tree survival in a tropical savanna in northern Australia. *Austral Ecology*, *24*(1), 50–59. https://doi.org/10.1046/j.1442-9993.1999.00946.x

Zepp, R. G., Miller, W. L., Burker, R. A., Parsons, D. A. B., & Scholes, M. C. (1996) Effects of moisture and burning on soil-atmosphere exchange of trace carbon gases in a southern African savanna. *Journal of Geophysical Research*, *101*(D19), 23699-23706. https://doi.org/10.1029/95JD01371

Table 1. DALEC-GSI model parameter description and ranges allowed in the MCMC.

Parameter	Name	Range
f_{auto}	Autotrophic respiration fraction of GPP	0.3 – 0.7
f_{lab}	Fraction of GPP allocated to labile C pool	0.01 – 0.5
f_{fol}	Fraction of GPP allocated to foliage	0.01 – 0.5
f_{root}	Fraction of GPP allocated to fine roots	0.01 – 0.5
θ_{lab}	labile C turnover rate	10^{-5} – 10^{-1} d^{-1}
θ_{fol}	foliar C turnover rate	10^{-6} – 10^{-1} d^{-1}
θ_{roo}	fine roots C turnover rate	10^{-4} – 10^{-2} d^{-1}
θ_{woo}	wood C turnover rate	2.5×10^{-5} – 10^{-3} d^{-1}
θ_{lit}	litter C turnover rate	10^{-4} – 10^{-2} d^{-1}
θ_{som}	soil organic matter C turnover rate	10^{-7} – 10^{-3} d^{-1}
θ_{min}	litter mineralization rate	10^{-5} – 10^{-2} d^{-1}
Θ	temperature dependence exponent factor affecting litter and soil organic C turnover times	0.018 – 0.08
c_{eff}	canopy efficiency parameter	10 – 100
c_{lma}	leaf carbon mass per area	10 – 400 g C m^{-2}
VPD_{min}	optimal VPD for leaf production	1 – 5500 Pa
VPD_{max}	optimal VPD for leaf senescence	1 – 5500 Pa
Tmn_{min}	limiting Tmn for phenology	225 – 330 K
Tmn_{max}	optimal Tmn for phenology	225 – 330 K
$Photo_{min}$	limiting photoperiod for phenology	3600 – 82800 s d^{-1}
$Photo_{max}$	optimal photoperiod for phenology	3600 – 82800 s d^{-1}

Table 2. The terrestrial carbon budget of the pantropics retrieved in the FIRE and NOFIRE experiments during 2000-2015. We present mean annual values and the uncertainty across the 50% confidence range assuming spatial correlation between uncertainties in all pixels. All values are in Pg C y^{-1}, rounded to the first decimal. Negative values of NEE and NBE denote a net C uptake from the atmosphere.

Fluxes	FIRE: median (25^{th} / 75^{th} percentiles)[a]	NOFIRE: median (25^{th} / 75^{th} percentiles)
GPP	91.5 (83.5 /100.8)	91.3 (83.3 / 100.2)
Ra	47.4 (40.8 / 55.2)	47.5 (40.9 / 55.3)
NPP (GPP-R_a)	43.3 (36.8 / 50.7)	42.9 (36.4 / 50.1)
R_h	40.2 (33.1 / 48.5)	40.9 (33.7 / 49.1)
NEE (-NPP+R_h)	-2.9 (-6.7 / 1.0)	-1.9 (-5.5 / 1.9)
Fire emissions[b]	1.2 (0.9 / 1.5)	-
NBE (NEE+Fire)	-1.7 (-5.4 / 2.2)	-1.9 (-5.5 / 1.9)

[a]We assume spatial correlation between uncertainties in all pixels: the median, 25^{th} and 75^{th} percentiles represents the area-weighted aggregate of all pixels' median, 25^{th} and 75^{th} percentiles.

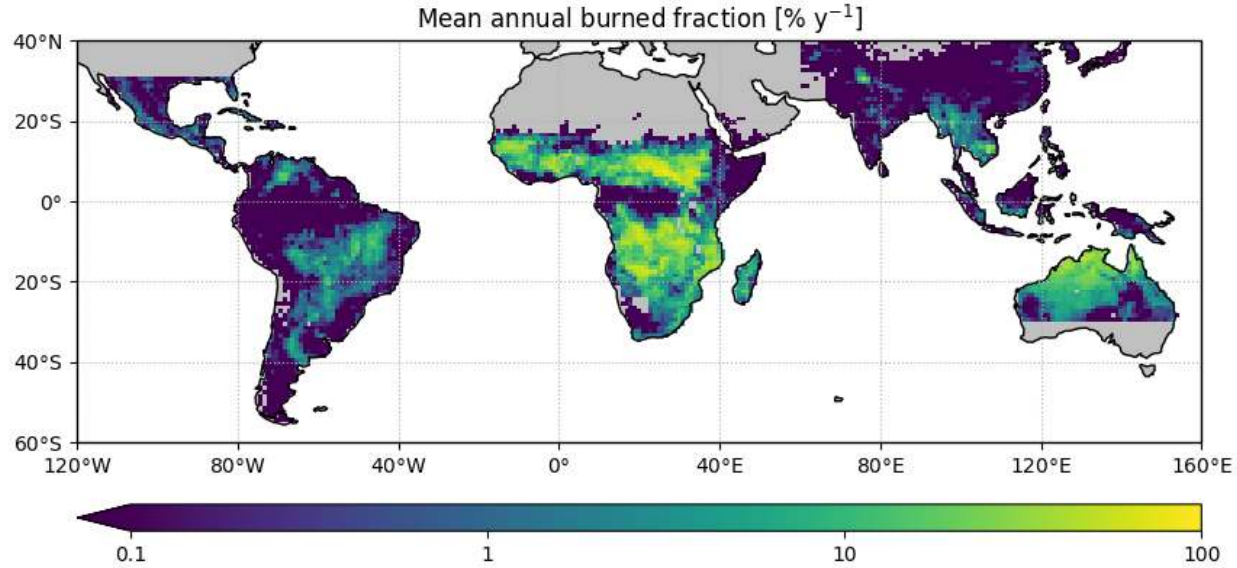

Figure 1. Mean annual burned fraction (%) derived from the GFED4 monthly database over 2000-2015 (Giglio et al., 2013). Data is represented for the study regions where equal amount of data were available to constrain CARDAMOM.

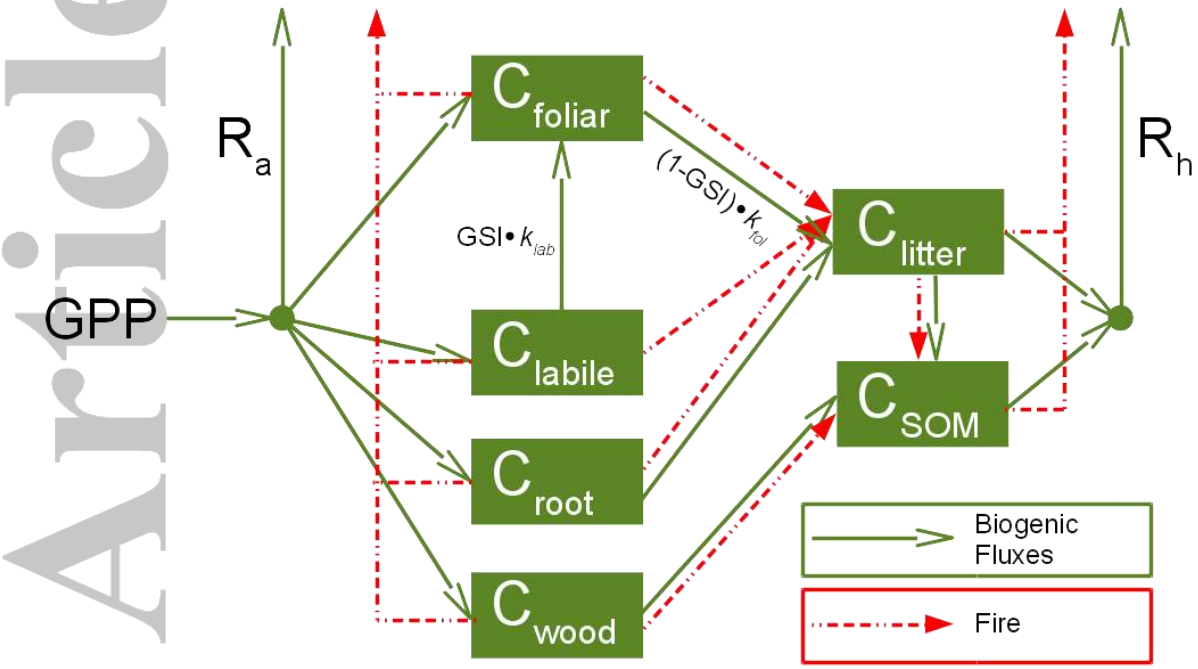

Figure 2. Schematic of the DALEC model. Green arrows represent biogenic fluxes between carbon pools. The build up of leaves from labile carbon (C_{labile}) is controlled by a Growing Season Index (GSI). Red arrows represent fire emissions (FE) and fire mortality (FM) fluxes which are calculated following equation 1 and 2 respectively.

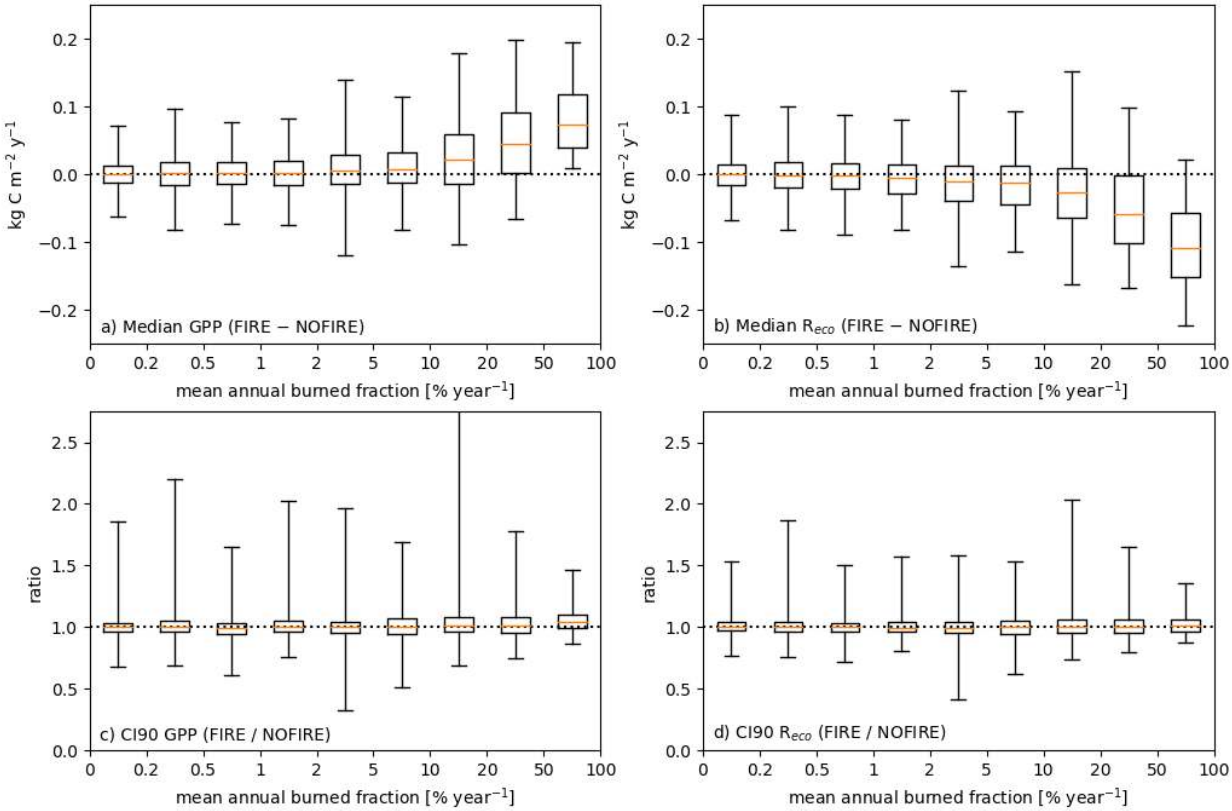

Figure 3. Impact of introducing fire on retrieved mean annual fluxes of GPP (a, c) and R_{eco} (b, d). The top row represents the absolute difference in the retrieved median values and the bottom row represents the relative difference in the spread of the CI_{90}.

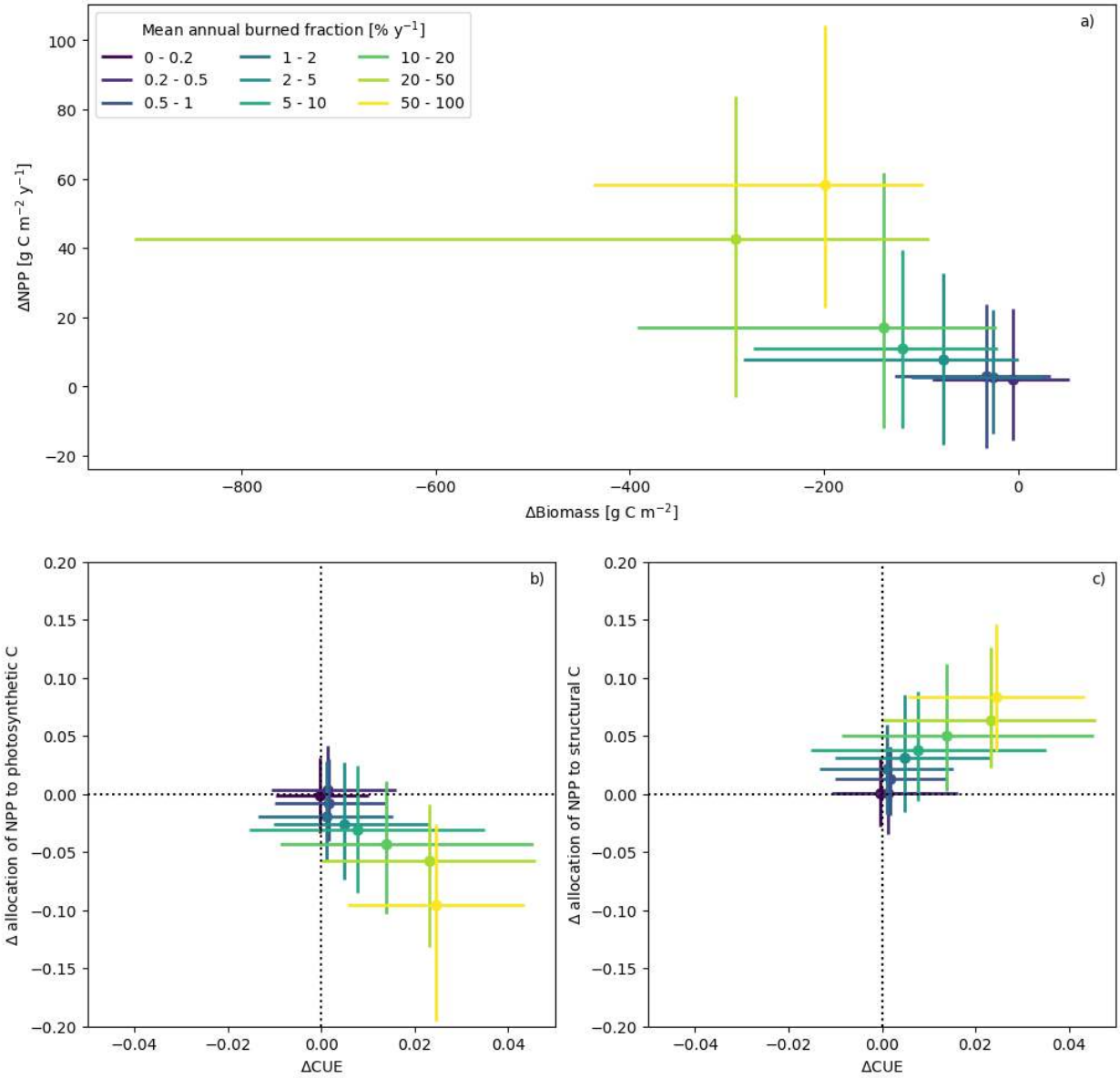

Figure 4. Difference in (a) retrieved NPP and biomass, (b) retrieved CUE and allocation of NPP to photosynthetic C and (c) retrieved CUE and allocation of NPP to structural C between the FIRE and NOFIRE experiments. Errors bars represent the 50% confidence interval of retrieved medians.

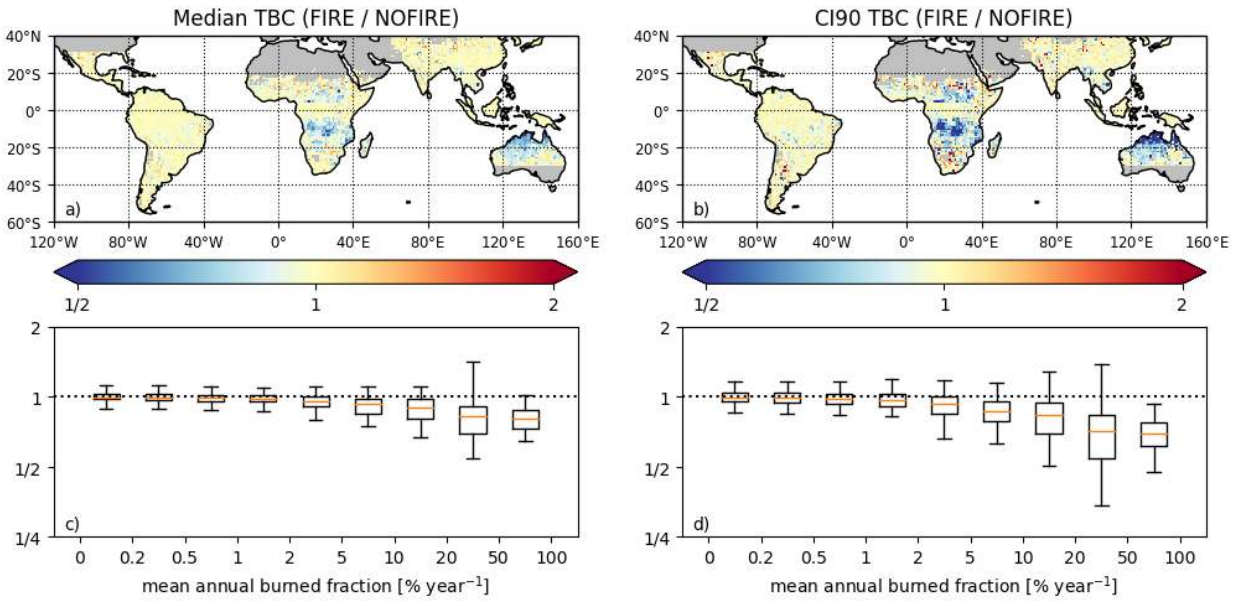

Figure 5. Ratio of total biomass carbon between FIRE and NOFIRE experiments. Ratio of median values (a) and ratio of the width of the 90% confidence interval CI_{90} (b) are presented. Panels (c) and (d) present the distribution of the information in maps (a) and (b) as a function of the mean annual burned fraction in each pixel, respectively. Boxes represent median and inter-quartiles while whiskers represent the 5th and 95th percentiles.

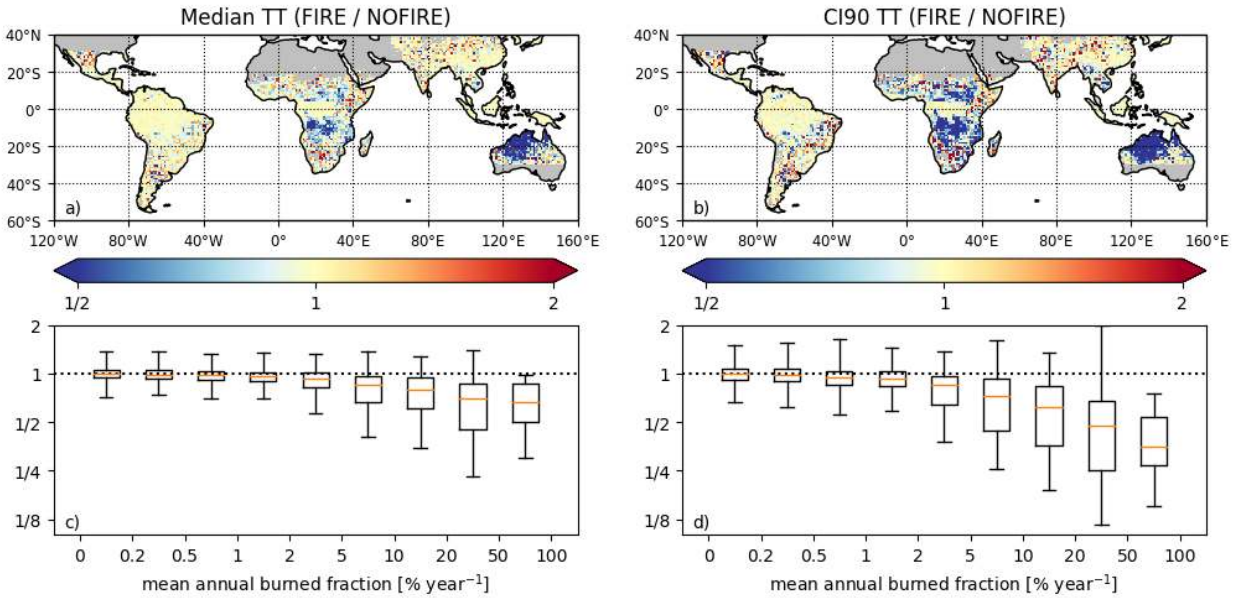

Figure 6. Ratio of vegetation carbon turnover times between FIRE and NOFIRE experiments. Ratio of median values (a) and ratio of the width of the 90% confidence interval CI_{90} (b) are presented. Panels (c) and (d) present the distribution of the information in maps (a) and (b) as a function of the mean annual burned fraction in each pixel, respectively. Boxes represent median and inter-quartiles while whiskers represent the 5th and 95th percentiles.